atmosphere

MDPI

Article

The 2018 Camp Fire: Meteorological Analysis Using In Situ Observations and Numerical Simulations

Matthew J. Brewer and Craig B. Clements *

Fire Weather Research Laboratory, Department of Meteorology and Climate Science, San José State University, San Jose, CA 95192, USA; mbrewerwx@gmail.com

* Correspondence: craig.clements@sjsu.edu; Tel.: +1-(408)-924-1677

Received: 5 December 2019; Accepted: 27 December 2019; Published: 29 December 2019

Abstract: The November 2018 Camp Fire quickly became the deadliest and most destructive wildfire in California history. In this case study, we investigate the contribution of meteorological conditions and, in particular, a downslope windstorm that occurred during the 2018 Camp Fire. Dry seasonal conditions prior to ignition led to 100-h fuel moisture contents in the region to reach record low levels. Meteorological observations were primarily made from a number of remote automatic weather stations and a mobile scanning Doppler lidar deployed to the fire on 8 November 2018. Additionally, gridded operational forecast models and high-resolution meteorological simulations were synthesized in the analysis to provide context for the meteorological observations and structure of the downslope windstorm. Results show that this event was associated with mid-level anti-cyclonic Rossby wave breaking likely caused by cold air advection aloft. An inverted surface trough over central California created a pressure gradient which likely enhanced the downslope winds. Sustained surface winds between 3–6 m s^{-1} were observed with gusts of over 25 m s^{-1} while winds above the surface were associated with an intermittent low-level jet. The meteorological conditions of the event were well forecasted, and the severity of the fire was not surprising given the fire danger potential for that day. However, use of surface networks alone do not provide adequate observations for understanding downslope windstorm events and their impact on fire spread. Fire management operations may benefit from the use of operational wind profilers to better understand the evolution of downslope windstorms and other fire weather phenomena that are poorly understood and observed.

Keywords: camp fire; fire weather; downslope windstorm; WRF; observations; doppler lidar

1. Introduction and Background

Many of California's largest, deadliest, and destructive wildfires occur during strong downslope windstorms. These strong and typically hot and dry downslope winds, which occur on the lee side of mountains, can be generically referred to as foehn winds [1,2]. Mountain waves and ensuing downslope windstorm dynamics have been observed and modeled extensively [3–8], among others. The basic conditions necessary for amplification of mountain waves, which lead to downslope windstorms, are strong winds between 7–15 m s^{-1}, flowing within 30° of perpendicular to the ridge line, and an inversion or layer of high static stability, located near crest height upstream of the mountain [5].

In California, these foehn winds are referred to by a number of different names. Most notably, Santa Ana winds (SAW) and Diablo winds (DW). SAW occur in Southern California during the fall, winter, and into spring, with occurrence peaking in December [9,10]. These winds are characterized by hot, gusty offshore winds, which promote the spread and ignition of wildfires. Mechanisms forcing SAW include a strong surface pressure gradient between coastal troughs and high-pressure systems over the Great Basin, as well as a temperature gradient between the cooler inland deserts and the coast [10,11]. Additional mid-level forcing for SAW includes 850 hPa cold air advection (CAA) and

negative vorticity advection at 500 hPa [12,13]. These hot, gusty conditions have fanned many large fires including, the Woolsey Fire in 2018, Thomas Fire in 2017, Witch Fire in 2007, and the 2003 Cedar and Old Fires [14]).

DW typically refer to the foehn winds that occur in the San Francisco Bay Area (SFBA) region, notable occurrences include the Wine Country/Napa county fires of 2017, specifically the Tubbs Fire, and the Tunnel Fire in the Oakland Hills in 1991 [15–17]. These winds are similar to SAW, with hot, dry, gusty downslope winds that predominantly occur in the fall [16,17]. Additionally, similar to SAW events, a DW forcing mechanism includes a coastal inverted trough and a high-pressure system in the Pacific Northwest or Great Basin regions of the Western United States [15,16]. The DW nomenclature has also been associated with the foehn wind in the western Sierra Nevada due to their similarities to the DW. However, the occurrence of foehn winds on the western Sierra Nevada does not mean that the DW will occur in the SFBA as well and vice-versa. Therefore, we classify downslope windstorms in the western Sierra Nevada as North winds following [2,18]. Additionally, we use North winds in this study to further differentiate between the two geographic regions of the SFBA and the Sierra Nevada and refer to this event as the downslope windstorm.

The Camp Fire ignited during a North wind event, which spread the fire rapidly and caused it to burn roughly 28000 ha in less than 24 h [19]. This North wind event brought gusts of over 15 m s^{-1} to the surface in an environment with record dry fuels. The Camp Fire was first reported at 06:33 PST 8 November 2018. The ignition was in the area of Camp Creek Road in the Feather River Canyon northeast of Pulga, CA [19]. Strong winds, >20 m s^{-1}, accelerated down the canyon likely contributed to both the start of the fire and rapid spread rate. The high rate of spread (ROS) pushed the fire through the communities of Concow, Paradise, and Magalia by the end of the day on 8 November 2018 destroying and damaging a majority of the buildings in its path. This extreme fire behavior can be largely attributed to the strong sustained and gusty winds and ember transport. The winds fanned the fire pushing the fire front at a high ROS, however, lofted fire brands may have been the main driver behind the high ROS. These fire brands were observed traveling distances of >1.5 km ahead of the main fire front causing spot fires and igniting many structures [20]. In total, the fire destroyed roughly 19,000 structures and had burnt roughly 62,000 ha once the fire was fully contained 17 days later on 25 November 2018 [19].

This downslope windstorm included aspects of both SAW and DW events. There are few, if any, examples in the literature of these downslope windstorms occurring in the western Sierra Nevada, especially regarding extreme fire weather. This case study of the meteorological conditions associated with the Camp Fire is motivated by the gap in the literature regarding this type of North wind event in addition to the magnitude of destruction associated with the fire. Results from this case study may be useful for forecasters in the private and public sector predicting these downslope windstorms for red flag warnings and power shut off programs.

This paper examines the meteorological context prior to and during the 2018 Camp Fire using both observations and numerical modeling. The structure of this paper is as follows: Section 2 describes the data and methods used in this analysis, Section 3 details the observed and modeled conditions prior to ignition as well as the conditions associated with the downslope windstorm event, Section 4 presents model verification metrics, and Section 5 summarizes the results and presents further discussion.

2. Data and Methodology

2.1. Observations

Many different observational datasets were used in this analysis of the conditions prior to and during the Camp Fire, including surface weather station observations, precipitation data, and remotely sensed observations. In order to assess the environment prior to the fire, we investigated October 2018 precipitation departures from climatology based off the climatological period of 1981–2010. These departures were made using the National Weather Service (NWS) advanced

hydrologic precipitation service quantitative precipitation estimate. The Stage IV precipitation data are quality-controlled, using radar and rain gauge estimates obtained from NWS River Forecast Centers and gridded by the National Centers for Environmental Prediction (NCEP) at 4 km resolution [21]. The climatological normal precipitation is derived from the parameter-elevation regressions on independent slopes model (PRISM) climate model data at 4 km grid spacing produced by the PRISM climate group at Oregon State University [22].

Surface in situ data were obtained from the United States Forest Service (USFS) remote automated weather station (RAWS) network and the Pacific gas and electric (PG&E) station network (Table 1). RAWS make up an interagency network of surface stations that are primarily used to assess fire danger in remote locations throughout the United States. RAWS are sited according to the National Wildfire Coordinating Group Standards for Fire Weather Stations and the National Fire Danger Rating System (NFDRS) protocol, with winds measured at 6.1 m (20 ft) AGL (above ground level) and the air temperature and relative humidity (RH) measured between 1.2–2.5 m (4–8 ft) AGL [23]. Wind and RH data are collected from 10 min averages prior to the hourly transmission time, while temperature is the instantaneous sample at the hour [23]. Site metadata and data collected from RAWS are used to calculate dead fuel moisture content. In this analysis, NFDRS 100-h fuel moisture content (FM-100) was used to investigate fuel moisture prior to ignition [24]. This fuel class represents dead fuels that take 100 h to reach 2/3 of equilibrium with the local environment, and range in size from 25 mm to 75 mm [25]. FM-100 were chosen due to their slower response time, which shows larger scale variations in the weather, and for the size of the fuel class. In total, five RAWS, (Jarbo Gap, Openshaw, Colby Mountain, Saddleback, and Humbug) and two PG&E weather stations, (Stirling City and Red Hill Lookout) were used in this analysis, and station locations are shown in Figure 1B. In order to assess the climatology of FM-100, the entire record of each RAWS was used to calculate daily minimum and average FM-100 and compared to daily FM-100 from 1 October 2018 through 10 November 2018. The time span from 00:00 PST 7 November 2018–00:00 PST 10 November 2018 was used to analyze the downslope windstorm conditions. Additionally, a sounding from the NWS in Reno, Nevada was obtained for 12:00 UTC 8 November 2018 [26].

Table 1. Description of weather stations used in this analysis.

Station Name	Station ID	Lat/Lon	Elevation (m)	Type	Record Span
Jarbo Gap	JBGC1	39.74, −121.49	773	RAWS	2003/04/21–Current
Openshaw	CICC1	39.59, −121.64	82	RAWS	1999/12/02–Current
Saddleback	SLEC1	39.63, −120.86	2033	RAWS	2001/06/26–Current
Colby Mtn.	CBXC1	40.14, −121.52	1830	RAWS	2015/06/08–Current
Humbug Summit	HMRC1	40.11, −121.38	2046	RAWS	2012/07/24–Current
Stirling City	PG131	39.91, −121.53	1143	PG&E	2018/10/02–Current
Red Hill Lookout	PG129	40.03, −121.18	1930	PG&E	2018/10/11–Current

In conjunction with surface in-situ observations, this analysis takes advantage of remotely sensed observations from lidar and radar. The California State University Mobile Atmospheric Profiling System (CSU-MAPS) [27] was deployed to the Camp Fire on 8 November 2018. The CSU-MAPS was equipped with a Halo Photonics, 1.5 µm scanning Doppler lidar, which has a resolution of 18 m and a range of 9.6 km. The lidar records attenuated backscatter and Doppler radial velocity data, as well as vertical wind profiles. Vertical wind profiles near the fire front were measured at two locations (Figure 1B). Location one was along Pentz Road on the southern flank of the fire and location two was located at the temporary incident command post at Butte College, also roughly on the southern flank. Radar data from the smoke plume were obtained from the KBBX Beale Air Force Base, California NWS next-generation radar (NEXRAD) weather surveillance radar-1988 Doppler (WSR-88D) S-band radar for 8–9 November 2018 (Figure 1B) [28]. Data from both the lidar, radar, and surface stations are used in this analysis to validate model simulations and assess fire risk.

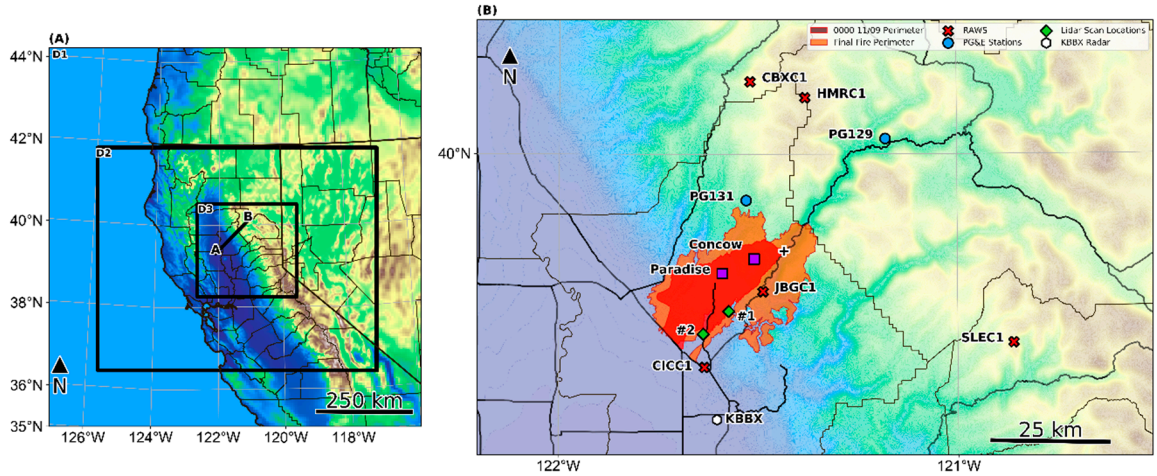

Figure 1. (**A**) Domains used in weather research and forecasting (WRF)-advanced research WRF (ARW) simulations and topography shaded. Outer domain D1 has a grid spacing of 6 km, with inner domains D2 and D3 grid spacing of 2 km and 0.666 km, respectively. Line AB represents the cross-section used in this analysis; (**B**) WRF model terrain (shaded) with locations of remote automated weather station (RAWS) (Xs), Pacific gas and electric (PG&E) stations (circles), lidar scan locations (diamonds), KBBX radar (hexagon), approximate ignition point ("+"), and city locations (squares). Shaded in red are Camp Fire perimeters with the inner perimeter from 00:00 PST 9 November 2018 and the outer perimeter being the final perimeter.

2.2. Modeled Data

The analysis of synoptic weather patterns prior to and during the Camp Fire were made using the global forecast system (GFS) analysis products from NCEP at 0.5° grid spacing 7–9 November 2018 [29]. The GFS was chosen due to its widespread use in operational fire weather forecasts in the United States. We used the GFS data to investigate the mid-level synoptic evolution at 700 hPa, this level was analyzed due to being just above crest height throughout much of the Sierra Nevada. The specific products analyzed at 700 hPa include geopotential heights, temperature, wind, and temperature advection. Additionally, the surface conditions were analyzed using mean sea level pressure (MSLP). These products give insight on the synoptic driver behind the North wind event that occurred in the western Sierra Nevada on 8 November 2018.

In addition to the GFS, a high-resolution simulation was used to analyze fine-scale winds, specifically the wind structure associated with the downslope windstorm. The simulation was made using version 4.0 of the weather research and forecasting (WRF) model's advanced research WRF (ARW) core [30]. WRF simulation utilized 2-way nesting for three nested domains with grid spacing of 6 km, 2 km, 0.666 km, and 80 vertical levels; the domains with respective grid spacing are shown in Figure 1A. The simulation was integrated for 48 h from 00:00 UTC 8 November 2018–00:00 UTC 10 November 2018, with initialization and boundary conditions from the 12 km NCEP North American Mesoscale model [31]. Table 2 lists WRF model physics parameterizations used in this simulation. Consistent with [32–34], we tested a number of different physics configurations, including a HRRR-like setup, but found that the combination of the Pleim-Xiu land surface model and the Asymmetric Convection Model version 2 (ACM2) PBL scheme performed best overall (not shown) [35,36]. Additionally, this analysis compared WRF 10 m wind speed and direction directly to 6.1 m RAWS wind observations. We decided to not adjust the wind measurements from 10 m to 6.1 m due to the fact that operational weather models typically only report 10 m winds and recent studies [31,33] found that adjusting measurements lower had little effect on results.

Table 2. WRF model parameterization name and namelist option.

Parameterization Type	Physics Scheme
Microphysics	Thompson graupel (8)
Radiation	RRTMG (4)
Surface layer physics	Pleim-Xiu (7)
Planetary Boundary Layer	ACM2 (7)

3. Results

3.1. Precipitation and Fuels

Live and dead fuels typically reach their minimum in fuel moisture content (FMC) in the fall, September–October, due to the lack of precipitation, high temperatures, and low RH experienced throughout the summer. FMC start to recover in the late fall as precipitation, lower temperatures, and higher RH become more common. However, a lack in precipitation throughout October of 2018 led to departures from the long-term climatological normal of 50–100 mm of precipitation in the area of the Camp Fire (Figure 2). The lack in precipitation during the month of October led to continued drying of fuels in the region. The only precipitation occurred between 3–5 October, when the FM-100 at all RAWS reached a relative maximum and declined through 25 October (Figure 3). Between 25–30 October 2018, an increase in RH (not shown) led to increased FM-100 (Figure 3). Throughout the remainder of October and into November, leading up to the ignition of the fire, no precipitation or prolonged high RH was measured at any of the nearby RAWS sites. This lack of precipitation and lower RH led to all RAWS station reaching within 0.5% of their lowest calculated FM-100 in the stations recording period, prior to the fire and through 10 November 2018 (Table 1). The average FM-100 on the day of ignition was 4.88%, with the lowest FM-100 tied between Openshaw and Colby Mountain RAWS of 3.8%.

3.2. Synoptic Overview

The mid-level evolution of geopotential heights, winds, and temperature advection from 10:00 PST 7 November 2018–10:00 PST 9 November 2018 is shown in Figure 4A–E. Figure 4A shows an amplified ridge extending well into British Columbia, Canada, which created northerly flow along the Canadian and United States west coast advecting colder air into the region over southwest Oregon and northwest California. Twelve hours later (Figure 4B), a short-wave trough became embedded within the larger ridge over northern California, which was likely caused by the height falls associated with the cold air advection (CAA) in the layer. This persistent CAA continued to deepen the shortwave trough and erode the base of the ridge, potentially contributing to anticyclonic Rossby wave breaking (AWB) as the CAA continued to deepen the shortwave and tilt the ridge (Figure 4C). Rossby wave breaking can be defined by the irreversible deformation of potential vorticity (PV) contours on isentropic surfaces over a longitudinally confined region, which are associated with stratospheric PV streamers intruding the troposphere [37–39]. Near the start of the AWB event at 10:00 PST 8 November 2018, there is a longitudinal gradient >5 PVU along the 120° W meridian on the 330 K isentropic surface, consistent with a high PV streamer intrusion (not shown). The shortwave trough and the AWB at 700 hPa aligned the winds with the Sierra Nevada ridge crest. This cross-barrier flow of 7–10 m s^{-1}, roughly at crest height, is one of the basic requirements that led to downslope windstorms. An inversion located roughly near crest top is shown in the 120:0 UTC 8 November NWS Reno, NV sounding, which indicates the last basic requirement for downslope windstorms to occur (Figure 5). The combination of these conditions likely led to the strong, gusty winds of >20 m s^{-1} experienced throughout much of the western slopes of the Sierra Nevada.

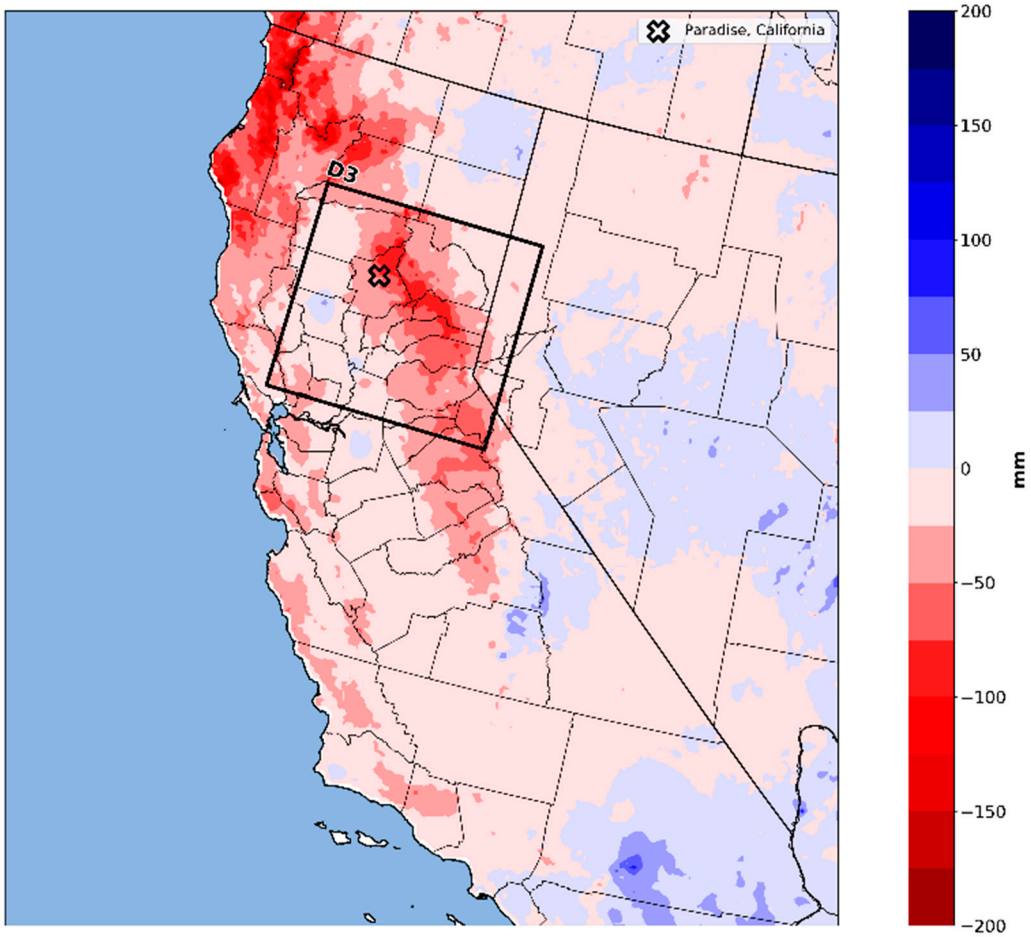

Figure 2. National Weather Service (NWS) advanced hydrologic precipitation service quantitative precipitation estimate departures from normal based on 1981–2010 climatology.

At the surface, an inverted trough provided additional forcing, enhancing the downslope winds (Figure 6). GFS MSLP for 04:00 PST 8 November 2018–10:00 PST 9 November 2018 are shown in Figure 6A–E. The large pressure gradient between the surface high in eastern Oregon and northern Nevada combined with the inverted surface trough in the Central Valley of California, acted to increase near-surface wind speeds, especially in areas where gap flow occurred through mountain passes (Figure 6A). The Feather River Canyon likely funneled these gap winds, similar to that experienced during SAW events in southern California [10,11]. The strong flow down the canyon was exacerbated by the already high winds associated with the synoptic-scale forced winds. The strong pressure gradient was persistent throughout the day on 8 November and into the evening (Figure 6C,D). However, aloft at 700 hPa, the geopotential height gradient, winds, and CAA continued to weaken throughout the night on 8 November 2018 as the shortwave and AWB crest continued to propagate southeast across the southwest US (Figure 4D). By the morning of 9 November 2018, the pressure gradient at the surface weakened considerably, while aloft the winds became calm–~5 m s^{-1} with flow roughly parallel with the Sierra Nevada crest (Figures 4E and 6E). On 9 November 2018, the large-scale weather pattern, which was forcing the downslope windstorm, had subsided and caused the surface winds to weaken.

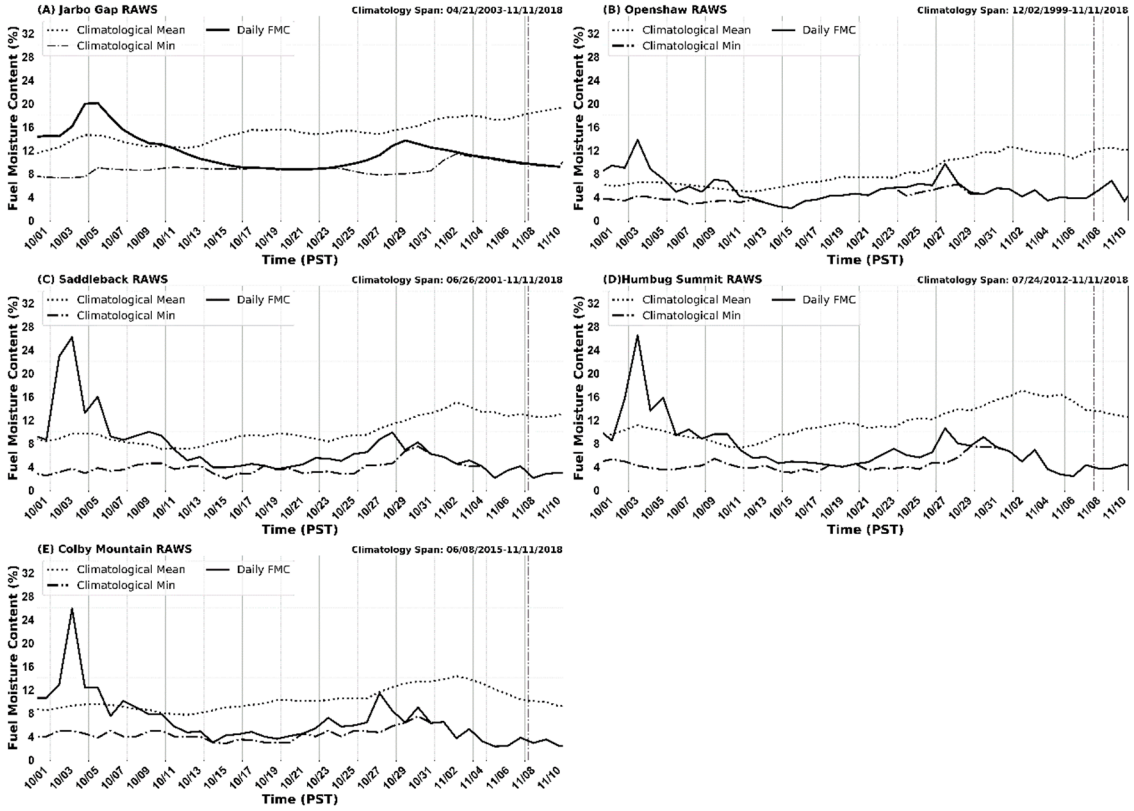

Figure 3. Calculated FM-100 for RAWS in the area surrounding the Camp Fire. Solid line indicates fuel moisture content (FMC) at the date shown in 2018, dashed line indicates recorded minimum FMC, dotted is daily average for recorded period. Vertical dashed line indicates approximate ignition time. Table 1 gives the climatological record for each station.

3.3. Observations

In situ weather observations in the area of the Camp Fire were made primarily from various surface weather stations within a roughly 60 km radius from Paradise, CA (Figure 1B, Table 1). The Jarbo Gap RAWS (Figure 7A) typically experiences moderate NE drainage winds at night and weak WSW upslope flow during the day time, which is likely caused by local topography of the Feather River Canyon and the Sierra Nevada. However, due to the synoptically forced downslope gap winds, the station experienced very strong NE winds throughout the night of 7 November and into the morning on 8 November 2018, with sustained winds over 12 m s^{-1} and gusts over 23 m s^{-1}. During the day on 8 November 2018, the winds were moderate with sustained winds between 3–8 m s^{-1} and gusts up to ~15 m s^{-1}. Wind speed and gusts increased in magnitude into the evening of the 8th and were steady into the morning of the 9th. After 06:00 PST 9 November 2018, the data at Jarbo Gap became questionable because based off observations of soil temperatures > 40 °C and erratic winds, the station may have been burnt over or fire was very close in the time period near 08:00. However, the station did record the daytime winds switching to the WNW weak upslope that would be expected with a lack of synoptic forcing influencing the winds.

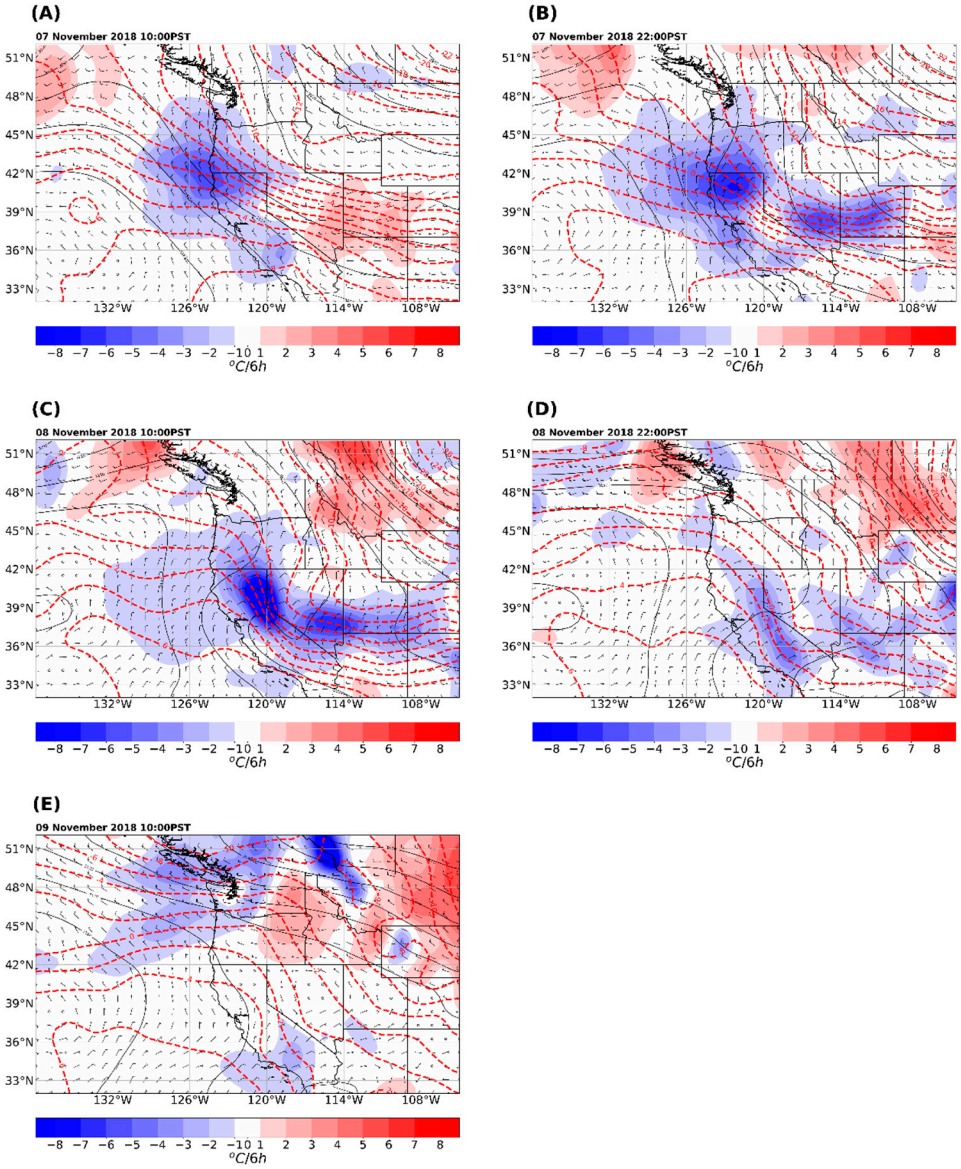

Figure 4. 0.5° National Centers for Environmental Prediction (NCEP) global forecast system (GFS) analysis at 700 hPa with geopotential heights in black contours, temperature in red dashed contours, temperature advection in color fill, and wind in barbs. (**A**) shows the analysis at 10:00 PST 7 November 2018, each subsequent figure (**B**–**D**) is 12 h later, ending at 10:00 PST 9 November 2018 (**E**).

The Openshaw RAWS (Figure 7B), which is located more in the California Central Valley, experienced strong NW flow, with gusts of ~13 m s^{-1}, likely caused by the strong inverted surface trough. At 17:00 PST 8 November 2018, the wind direction switched to NNE with gusts of ~10 m s^{-1}, suggesting that the downslope winds were able to push farther down the slope and into the valley. The strong downslope winds that pushed into the valley were likely a factor that allowed the fire to progress to and even cross CA Highway 99, a wide four-lane highway (Figure 1B and [19]). Colby Mountain, Humbug Summit, and Saddleback RAWS all experienced similar downslope windstorm conditions, with NE and ENE winds and peak gusts occurring in late morning of the 8th. Both Colby Mountain and Saddleback RAWS recorded gusts > =26 m s^{-1} with early sustained winds >=10 m s^{-1}. Humbug Mountain RAWS did not experience as strong of winds, with gusts of ~14 m s^{-1} and sustained winds of ~5 m s^{-1}, but these data still indicate the presence of downslope winds.

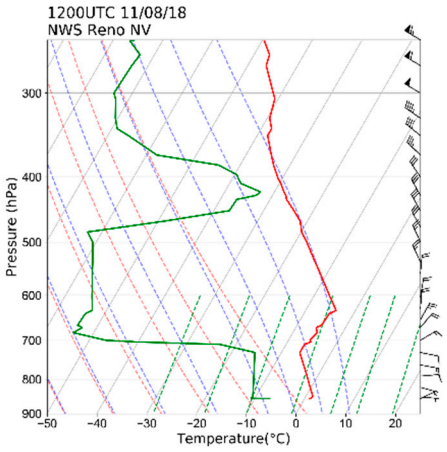

Figure 5. NWS Reno Nevada 12:00 UTC 8 November 2018 sounding.

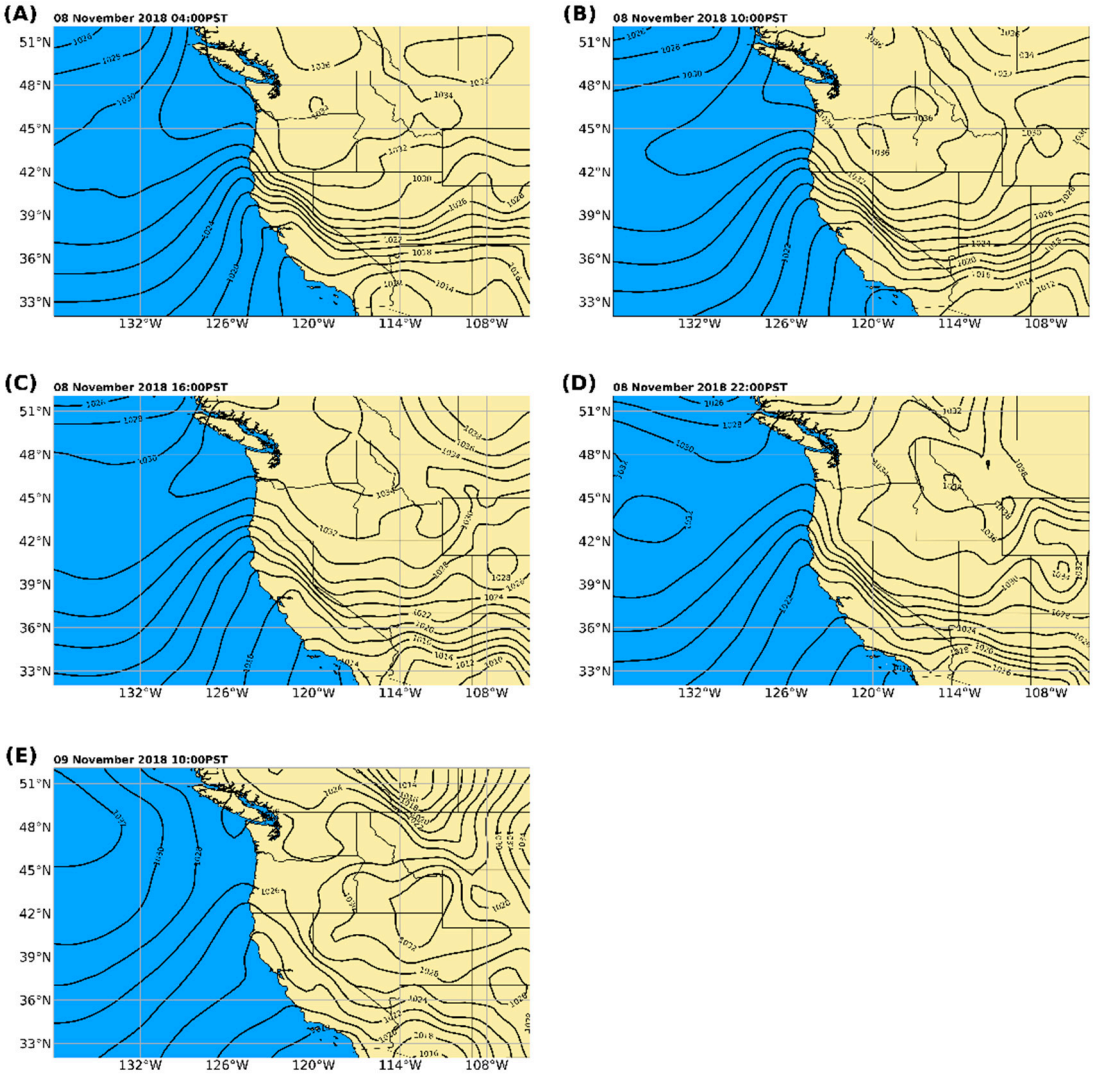

Figure 6. 0.5° NCEP GFS analysis with mean sea level pressure (MSLP) in black contours. (**A**–**D**) show the analysis from 04:00 PST 8 November 2018 through 22:00 PST 8 November 2018, every 6 h. (**E**) shows the analysis 12 h later at 10:00 PST 0 November 2018.

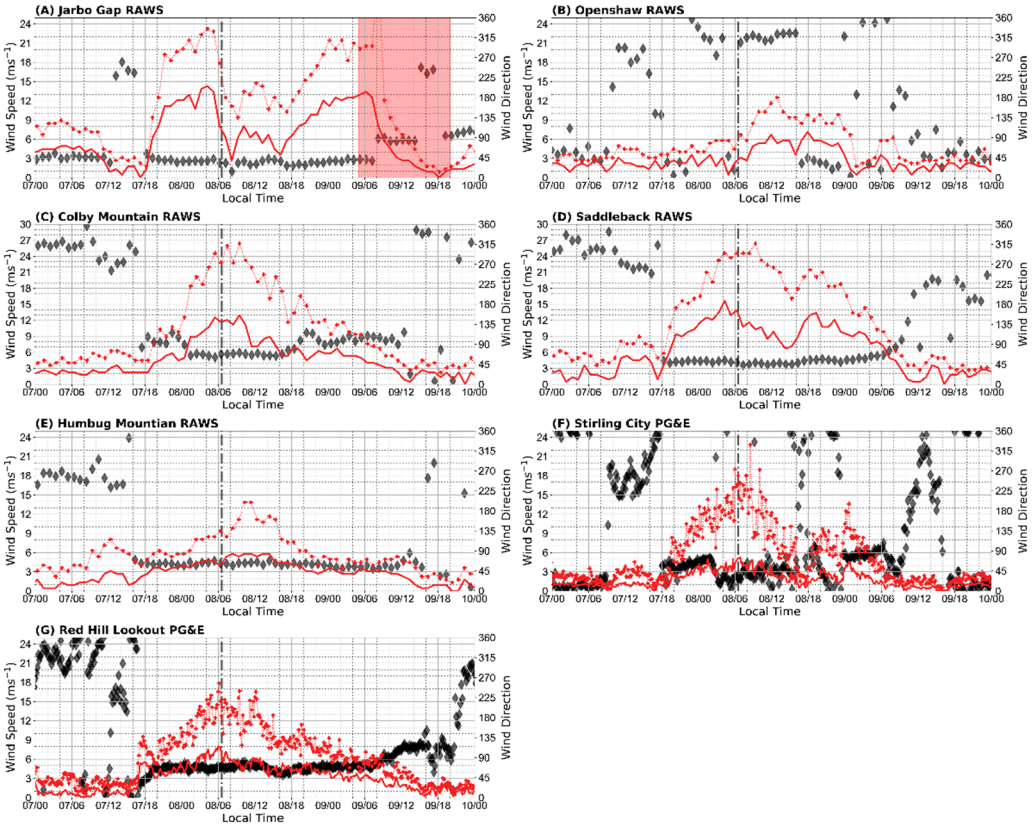

Figure 7. Time series of wind speed (red) and wind direction (black diamonds), and gusts (red dashed line and "+") for each weather station, (**A**) Jarbo Gap RAWS, (**B**) Openshaw RAWS, (**C**) Colby Mountain RAWS, (**D**) Saddleback RAWS, (**E**) Humbug Mountain RAWS, (**F**) Stirling City PG&E, (**G**) Red Hill Lookout PG&E. The approximate ignition time is indicated by vertical dashed line. The red box in (**A**) indicates period of questionable data as denoted by Mesowest.

The Red Hill Lookout PG&E station observed similar conditions to that of Humbug Mountain, with ENE wind direction and extremely steady sustained winds of ~6 m s^{-1}, which began to taper off at 00:00 PST 9 November 2018. This station experienced strong gusts peaking at 18 m s^{-1} roughly at the time of ignition and tapering off similar to the sustained winds. The Stirling City PG&E station observed the strong ENE–NNE downslope winds throughout the night and morning on 8 November 2018. However, after 12:00 PST 8 November, the winds weakened and became more variable. The station experienced two periods of weak SE flow followed by stronger NNE winds, which may indicate that this station was located either underneath a rotor in the downslope winds or is poorly sited.

The deployment of the CSU-MAPS truck to the Camp Fire allowed for observations of the vertical structure of the wind. Figure 1B shows the two lidar scanning locations, which at the scan times, were approximately along the southern flank of the fire. Vertical wind profiles from the lidar are shown in Figure 8. Figure 8A shows what appears to be an intermittent low-level jet located just above the surface between 100–400 m AGL, with a separate wind maximum between 400–700 m AGL. The wind direction at the surface was northeasterly, which tended to veer eastward with height (Figure 8A). At the second scan location, Figure 8B, the winds were stronger throughout the profiles and the wind speeds tended to increase with height. Again, in this profile, the wind directions veered with height from NNE to E. Both sets of profiles show moderate winds, on the order of ~8 m s^{-1}, located just above the surface with lidar-observed boundary-layer heights of 800−1000 m AGL (not shown). These winds aloft continued to allow for the transport of firebrands in addition to increasing ROS along ridgelines and hilltops in the lower foothills to the southwest of Paradise. It should be noted that the surface winds, at the time the wind profiles were made, were weaker and so while winds at the surface were

not very strong, the winds aloft were. The winds aloft mixed down to the surface bringing higher momentum from aloft to the surface, which also helps drive ember transport.

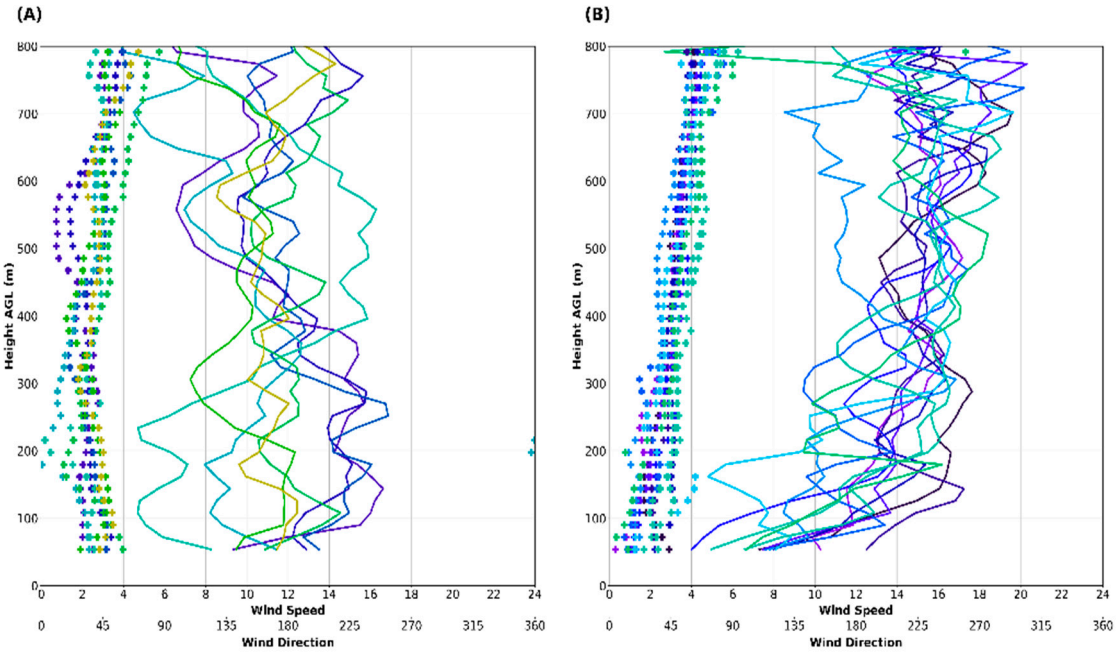

Figure 8. (**A**) Observed lidar vertical wind profiles from scan location #1 (Figure 1B). Wind speed (m s^{-1}) is represented by the solid lines with "+" representing the corresponding wind direction (°). Each color represents the profile taken every 5 min between 19:00–19:40 PST 8 November 2018. (**B**) Lidar vertical wind profiles from scan location #2 (Figure 1B) with wind speed represented by the solid line with "+" representing associated wind direction. Each color represents the profile taken every 5 min between 21:00–22:00 PST 8 November 2018.

3.4. WRF Analysis

Radar observations of the smoke plume were available due to the proximity of the KBBX radar. Figure 9A–E shows the evolution of both the fire and the surface winds using the base radar reflectivity and the 2 km resolution WRF 10 m winds. The 07:21 PST 8 November 2018 radar scan (Figure 9A) was the first scan time that the smoke plume became visible within the ground clutter. The next scan (Figure 9B) at 07:46 PST 8 November 2018 clearly shows the smoke plume boundaries in the reflectivity, which was aligned NE with the strong model winds. By 11:27 PST 8 November 2018 (Figure 9C), the large ash and smoke particles extended ~70 km from the base of the plume. The plume axis was still in line with the NE downslope winds, even as the plume extended over the NW surface flow in the Central Valley. Additionally, the reflectivity origin in the area of Paradise, CA resembled what may have been the fire front structure. This shape is similar to many wind-driven fire fronts with the center of the fire being spread faster as a head fire by the wind than the flanks, thus creating an elongated "U" shape in the reflectivity (e.g., [40,41]). This feature in the reflectivity persisted throughout much of the day. Figure 9D shows another example of this reflectivity structure and how the modeled winds are aligned with the plume and estimated fire front structure. As the fire continued to burn into the evening on 8 November 2018 (Figure 9E,F), the smoke plume boundaries became wider as the fire's flanks continued to burn outward, however the "U" shape in the fire front structure was still somewhat apparent. Additionally, the highest reflectivity in the smoke was coming from the area of Paradise, CA and was likely due to more ash particles and larger debris associated with many structure fires.

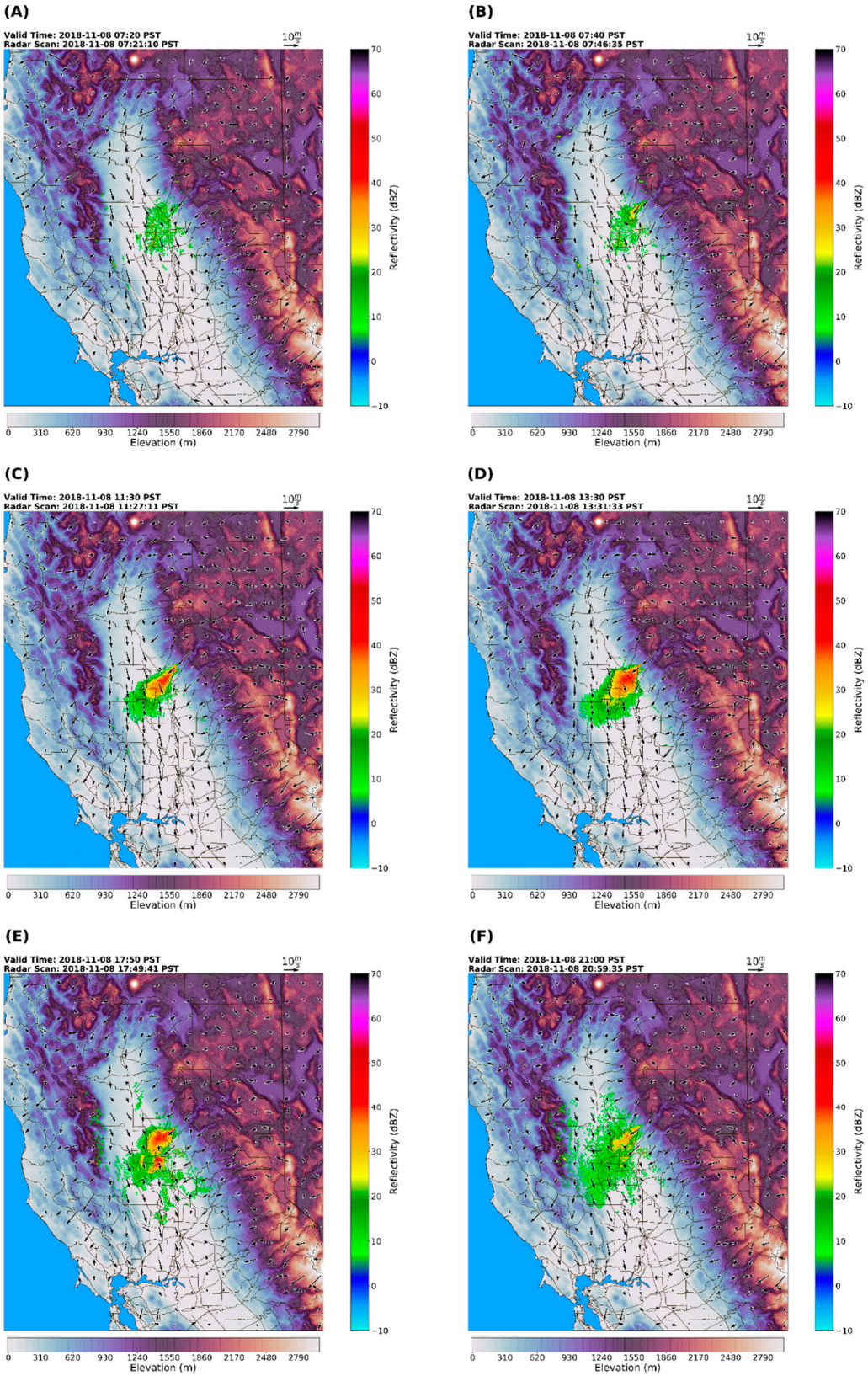

Figure 9. KBBX radar base reflectivity, WRF D2 terrain and 10 m winds (vectors). Radar scan times are plotted with the nearest WRF output times of 07:20, 07:40, 11:30, 13:30, 17:50, and 21:00 PST 8 November for subplot (**A**), (**B**), (**C**), (**D**), (**E**), (**F**)**,** respectively.

In addition to using WRF to show the spatial extent of surface winds, cross sections of simulated wind and potential temperature were used to investigate the vertical structure of the winds and flow pattern associated with the downslope windstorm. At roughly the time of ignition, sustained winds above the surface and near the ignition point in Concow, CA were >25 m s^{-1} (Figure 10A). Additionally, Figure 10 illustrates typical flow for a downslope windstorm with the subcritical flow upstream of the crest, which becomes supercritical accelerating down the lee of the Sierra Nevada creating multiple hydraulic jump structures [5,7]. The synoptic features discussed above, in addition to the surface observations, suggest that this simulated downslope windstorm is realistic. The strongest winds had a tendency to stay in the higher elevations near the crest, but winds of 10–20 m s^{-1} just above the surface were present throughout much of the day in the area of Concow and Paradise (Figure 10B,C). The downslope winds continued into the evening of 8 November 2018 as shown in Figure 10D, however as mid-level support waned, the winds likely were driven by nocturnal drainage flow combined with the pressure gradient between the Great Basin and the Central Valley. The combination of output from operational atmospheric models, surface observations, observed vertical wind profiles, and this WRF simulation, show that the strong winds associated with the Camp Fire were likely caused by a downslope windstorm and gap-flow winds. Additionally, these strong winds combined with extremely low fuel moistures created a very dangerous environment that was primed for extreme fire behavior.

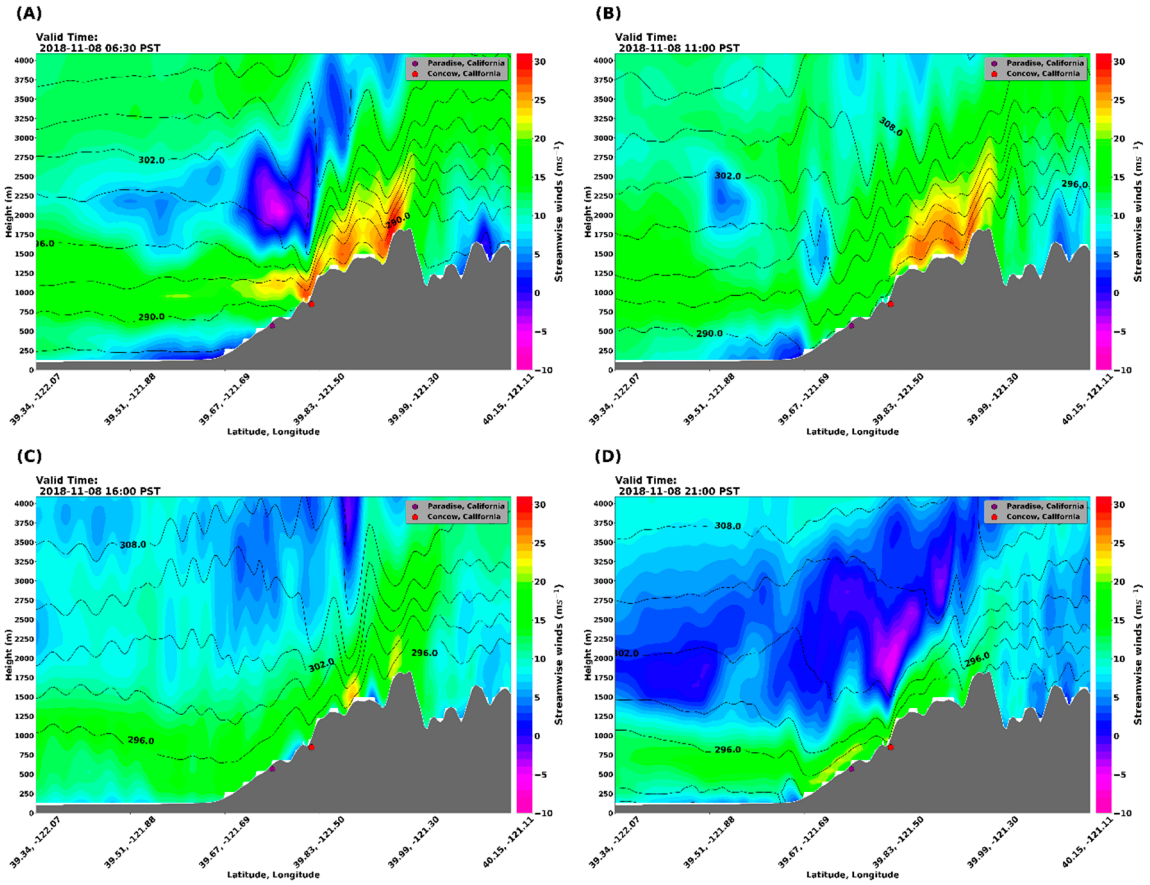

Figure 10. WRF D3, 0.666 km resolution vertical cross sections of streamwise winds (shaded), and potential temperature (contours) at 06:30, 11:00, 16:00, and 21:00 PST 8 November 2018, subplots (**A**), (**B**), (**C**), and (**D**), respectively. The approximate locations of Paradise (hexagon) and Concow (circle) are also shown.

4. Model Verification

In order to assess how WRF simulated the real atmosphere, we compared point forecasts for all weather stations used in this analysis, as well as vertical wind profiles analyzed against our lidar vertical wind profile observations. Figure 11 gives all stations wind speed and direction compared to WRF wind speed and direction averaged over the hour period. WRF modeled winds for each station were pulled from the grid box in which each station was located. The model both overestimated and underestimated winds at many of the locations, however at the Stirling City station, the model performed very poorly with averaged root mean square error (RMSE) of 6.77 m s^{-1}. Additionally, the model did not perform well forecasting wind direction at the Openshaw RAWS site. The model resolved NE downslope winds reaching the Openshaw station much earlier than what was observed. The RMSE wind speed and wind direction for all sites examined was 3.34 m s^{-1} and 54°, respectively. If the worst wind speed site, Stirling City, was removed, the RMSE would drop to 2.78 m s^{-1}, and if the worst wind direction site, Openshaw, was removed, the RMSE would decrease to 35°. Overall, Station observations versus WRF winds showed the simulation had a high bias compared to observations from both RAWS and PG&E stations, which may be caused by station siting, terrain influence, or measurement height differences (Figure 12). Furthermore, when comparing the RAWS against the model, the majority of points are above the 1:1 line, especially with regards to lower wind speeds (Figure 12A). However, there is much more spread in the wind speeds above 8 m s^{-1}. When comparing the PG&E stations to the model, there is a larger high bias (Figure 12B). Much of this high bias is likely from the Stirling City station, as well as the morning and midday of 8 November 2018 periods at Red Hill Lookout. However, the grouping of well modeled winds can be attributed to the evening of 8 November 2018 and the morning of 9 November 2018 at Red Hill Lookout (Figures 11G and 12B). Our WRF simulation made reasonable forecasts of the strong winds for the RAWS stations but failed at forecasting winds at PG&E stations.

In addition to the verification against surface stations, vertical lidar wind profiles were compared to WRF vertical wind profiles to assess how well the downslope winds aloft were simulated. Figure 13 shows the comparison of the two lidar scanning locations to the vertical profile of the nearest model grid location. The averaged modeled vertical profile and the averaged lidar wind profile were used to calculate RMSE. For both profiles, the model did not perform well. At location 1, the RMSE between modeled and observed wind speeds was 8.7 m s^{-1}. Additionally, the modeled and observed wind direction RMSE was 31.5°. The model predicted the wind direction well near the surface but resolved the shift in direction, from NE to E, at lower altitudes than what was observed. Lidar location 2 had a smaller RMSE of 4.77 m s^{-1}, which was likely due to the successful modeling of winds above 700 m AGL. The simulated wind direction at this location was also better with a RMSE of 16°. The wind profile at location 2 was simulated to be much closer to the observations with the model being able to better simulate both the change in wind direction with height and the wind speed profile. However, for both locations, the modeled wind direction had an easterly bias as compared to the observations.

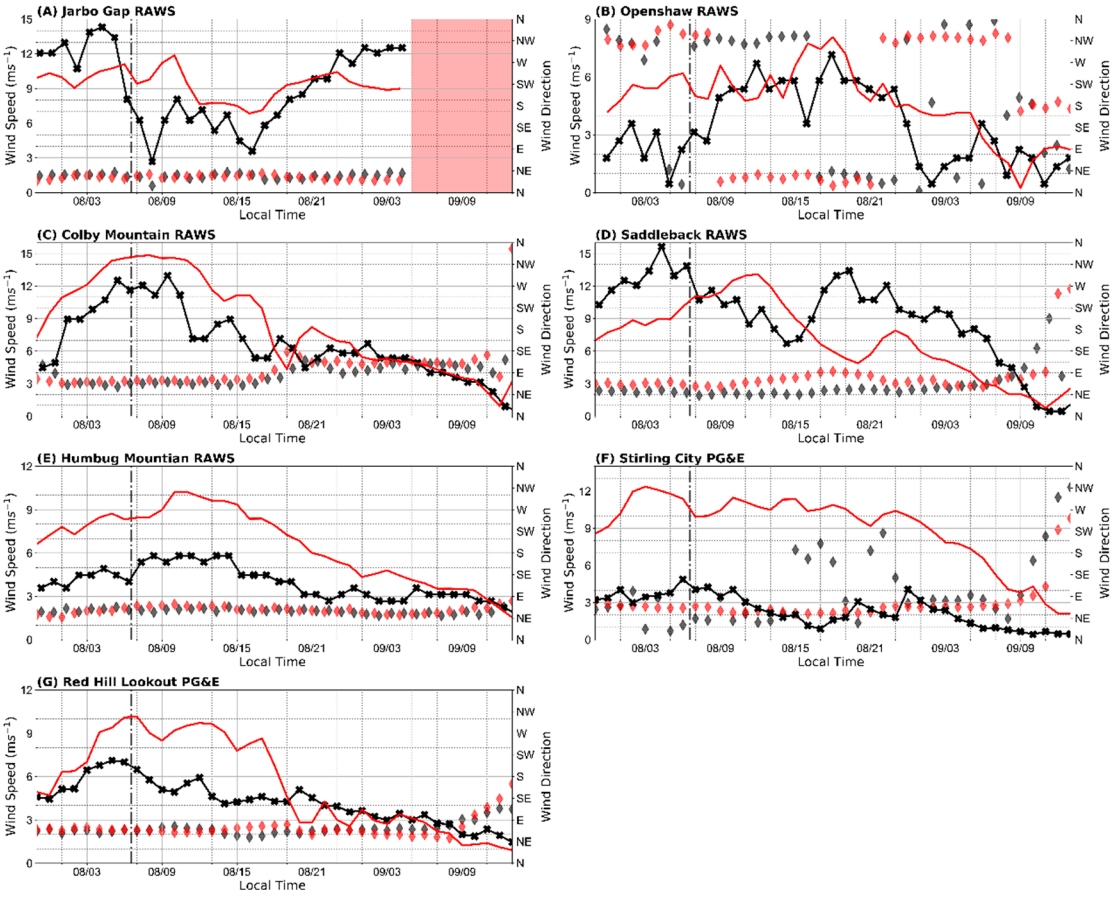

Figure 11. Time series of WRF 10 m wind speed (red lines) and direction (red diamonds) and the observed wind speed (black line with Xs) and direction (black diamonds) for each weather station (**A–G**) as in Figure 7. Dashed vertical line indicates approximate ignition time of the fire, and the red box in subplot (**A**) indicates where the station data are questionable and therefore omitted.

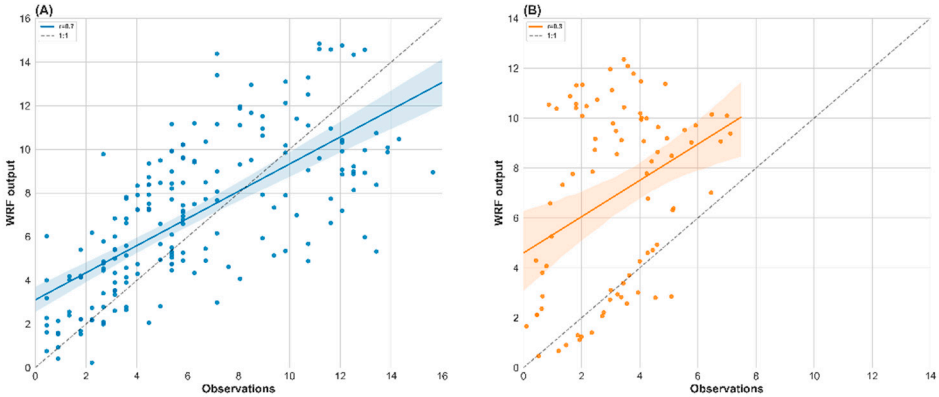

Figure 12. (**A**) WRF 10 m winds against RAWS stations, solid blue line indicates regression line and a 95% confidence interval (shaded), dotted line indicates 1:1. (**B**) WRF 10 m against Stirling City and Red Hill Lookout PG&E stations with regression line and confidence interval in orange.

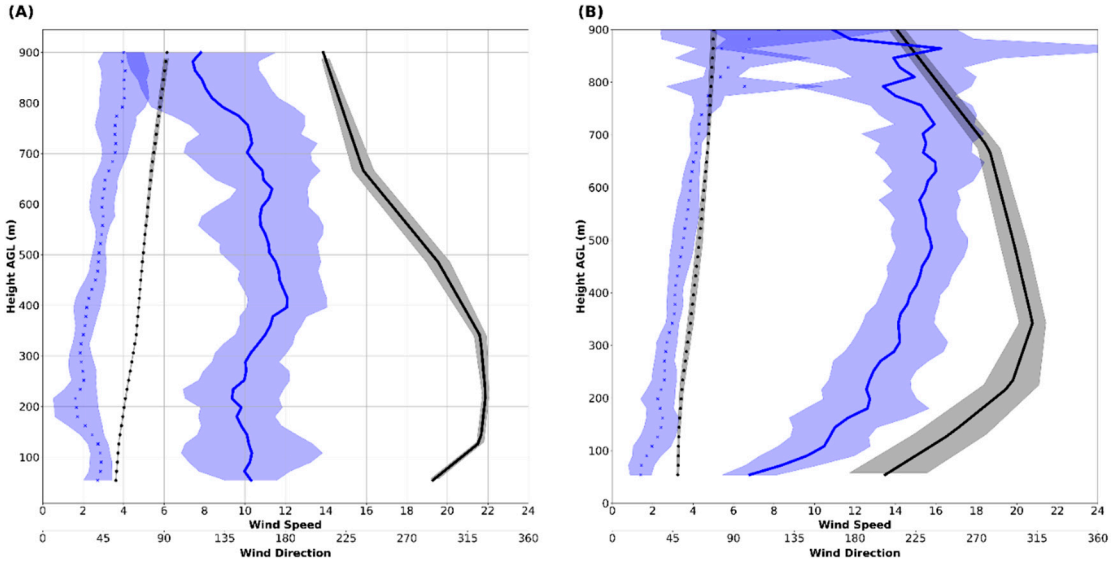

Figure 13. (**A**) Location #1 averaged lidar vertical wind speed (m s^{-1}) (blue line) and direction (°) (blue Xs). WRF modeled vertical wind speed (black line) and direction (black circles). Shading indicates ± 1 standard deviation. (**B**) Location #2 averaged lidar vertical wind speed (blue line) and direction (blue Xs). WRF modeled vertical wind speed (black line) and direction (black circles). Shading indicates ±1 standard deviation.

5. Discussion and Conclusions

The 2018 Camp Fire occurred during an episode of high-risk fire weather conditions. The lack of precipitation in the months leading up to ignition created an environment where calculated dead and live fuel moistures reached their record minimum. This environment alone had the potential to carry fire in the event of an ignition. The onset of a downslope windstorm from the evening on 7 November 2018 through the morning of 9 November 2018, created more critical conditions allowing for more rapid rates of spread, which caused the Camp Fire to be a fast moving and deadly wildfire event. A combination of synoptic events led to the development of the strong downslope windstorm. These events included the evolution of the mid-level atmosphere, which was caused by CAA potentially initiating and deepening a shortwave trough embedded within a high amplitude ridge. The amplified shortwave created flow perpendicular to the Sierra Nevada crest, and in addition to the presence of an upstream temperature inversion at crest level, provided the conditions needed for downslope windstorm development. Furthermore, surface pressure gradients throughout 8 November 2018 likely exacerbated the strong downslope winds. The pressure gradient between the California Central Valley and the Great Basin allowed for strong gap flow. This gap flow was particularly evident in the Feather River Canyon which recorded gusts of ~23 m s^{-1}. The synoptic-scale meteorological patterns associated with this event were similar to both DW and SAW events, but North wind events in the northern Sierra Nevada have, to date, not been thoroughly researched. Prediction of these windstorms is important for assessing fire danger especially for utility companies and preplanning for at-risk communities in the Sierra Nevada.

Observations from surface weather stations showed the presence of downslope winds associated with the event. RAWS and PG&E stations located near the Camp Fire recorded moderate to strong sustained winds between 5–15 m s^{-1} and gusts greater than 26 m s^{-1} during the first day of the fire, 8 November 2018. These winds were predominantly out of the NNE–E, indicative of typical downslope windstorms in the region. Doppler lidar observations made in the evening of 8 November 2018 indicated the presence of nearly constant and strong winds throughout the boundary layer, which were NE near the surface and veered with height to easterly aloft. The vertical wind profiles also indicated the presence of an elevated low-level jet structure intermittently. In addition to the

Doppler lidar observations, radar reflectivity of the smoke plume on 8 November 2018, indicated the wind-driven nature of the fire front and that the smoke plume was aligned from NE to SW along the predominant downslope wind direction. Observations in this study were able to verify that a downslope windstorm occurred. However, an increase in observations, both well-sited weather stations as well as lidar profilers, would be beneficial in providing real-time updates on the onset of these windstorms. Knowing when the onset of the strong wind occurs may be useful for utilities and local fire managers to be better prepared for future large wildfire events.

WRF simulations provided added context to the observations. For example, the simulations indicated that the vertical structure of the atmosphere throughout 8 November 2018 was indicative of a downslope windstorm. The simulated vertical cross sections of streamwise winds and potential temperature showed the presence of subcritical flow upstream of the ridgeline, which transitioned to the supercritical flow. The strongest winds in the simulation tended to be confined to higher elevations, but winds of over 20 m s^{-1} were not uncommon in areas further down the slope from Concow and Paradise. Additionally, the simulations revealed the presence of many hydraulic jump structures within the downslope windstorm, which may explain some of the observations of erratic winds at the Stirling City PG&E surface station. Furthermore, the hydraulic jump structures may be linked to intermittent gusty winds experienced on the ground and the lofting of fire brands during the fire.

Model performance when compared to observations varied. When compared to surface station observations, the model performed reasonably well with a strong correlation with RAWS, but an overall high bias was associated with weaker observed winds. When compared to the two PG&E stations, WRF performed poorly. The PG&E stations are not standardized, with instruments mounted at various heights with no information on heights or station placement. Due to the unknown placement of these sites and instruments, it is possible that the site is in an obstructed area or much closer to the ground. Additionally, due to the resolution of the model, there may have been subgrid-scale processes, such as lee-side rotors, that were not resolved in the simulations. Moreover, complex terrain may not be well resolved within the model, which may also affect how winds are simulated. When compared to lidar observed vertical wind profiles, WRF again had a high wind speed bias. This bias may be caused by the PBL parameterization resolving a characteristic log-wind profile that differed from the actual observations. These biases in WRF can be used by forecasters and fire managers to be able to better assess what the winds are doing on the ground, especially if they are utilizing a mesoscale forecasting model, such as WRF.

The Camp Fire event was one of the most devastating wildfires in California history. This event represents a case of extreme fire behavior associated with critically dry fuels and the onset of a downslope windstorm. The synoptic-scale meteorological conditions were well forecasted and the severity of the event was not surprising given the fire danger potential for that day. We show that our rapid-response deployment to that event provided a unique dataset not available through standard surface networks and that these data are necessary to evaluate the meteorological conditions at the fire front. However, our study does have some limitations that need to be mentioned here. One limitation of this study is that we do not describe the fire behavior in detail but focus primarily on the meteorological factors associated with the event rather than the fire evolution. Another caveat to our study is the we do not know how the atmosphere responded to the fire and whether or not our observed wind profiles were impacted by fire-induced circulations that may have formed in response to fire front heating. Finally, we want to point out that fire management operations may indeed benefit from the use of wind profilers, such as Doppler lidars, to better understand the evolution of downslope windstorms and other fire weather phenomena that are poorly understood and observed.

Author Contributions: Conceptualization, C.B.C.; formal analysis, M.J.B.; funding acquisition, C.B.C.; resources, C.B.C.; supervision, C.B.C.; visualization, M.J.B.; writing—original draft, M.J.B.; writing—review and editing, C.B.C, please turn to the CRediT taxonomy for the term explanation. Authorship must be limited to those who have contributed substantially to the work reported. All authors have read and agreed to the published version of the manuscript.

Funding: This research was supported by the National Science Foundation under award #1807774.

Acknowledgments: The authors want to acknowledge Jackson Yip for his participation in the field during the Camp Fire deployment, the Tahoe National Forest for sponsoring the team's red cards, and the funding provided by the National Science Foundation's Physical and Dynamic Meteorology Program, under award #1807774.

Conflicts of Interest: The authors declare no conflict of interest.

References

1. Brinkman, W.A.R. What is a Foehn? *Weather* **1971**, *26*, 230–240. [CrossRef]
2. Whiteman, C.D. *Mountain Meteorology, Fundamentals and Applications*; Oxford University Press: Oxford, UK; New York, NY, USA, 2000.
3. Klemp, J.B.; Lilly, D.K. The Dynamics of Wave-Induced Downslope Winds. *J. Atmos. Sci.* **1975**, *32*, 320–339. [CrossRef]
4. Smith, R.B. On Severe Downslope Winds. *J. Atmos. Sci.* **1985**, *42*, 2597–2603. [CrossRef]
5. Durran, D.R. Mountain Waves and Downslope Winds. In *Atmospheric Processes over Complex Terrain*; Meteorological Monographs; Blumen, W., Ed.; American Meteorological Society: Boston, MA, USA, 1990; Volume 23, pp. 58–81. [CrossRef]
6. Durran, D.R. Downslope winds. In *The Encyclopedia of the Atmospheric Sciences*, 1st ed.; Holton, J., Curry, J., Pyle, J., Eds.; Academic Press: Boston, MA, USA, 2004; pp. 644–650.
7. Cao, Y. The Santa Ana Winds of Southern California in the Context of Fire Weather. Ph.D. Thesis, University of California, Los Angeles, CA, USA, May 2015.
8. Markowski, P.; Richardson, Y. Mountain Waves and Downslope Windstorms. In *Mesoscale Meteorology in Midlatitudes*; Markowski, P., Richardson, Y., Eds.; John Wiley and Son: Hoboken, NJ, USA, 2010; pp. 327–348. [CrossRef]
9. Westerling, A.L.; Cayan, D.R.; Brown, T.J.; Riddle, L.G. Climate, Santa Ana Winds and Autumn Wildfires in Southern California. *Eos Trans. Am. Geophys. Union* **2004**, *85*, 289–300. [CrossRef]
10. Raphael, M.N. The Santa Ana Winds of California. *Earth Interact.* **2003**, *7*, 1–13. [CrossRef]
11. Edinger, J.G.; Helvey, A.R.; Baumhefner, D. *Surface Wind Patterns in the Los Angeles Basin during Santa Ana Conditions*; Department of Meteorology, UCLA: Los Angeles, CA, USA, 1964.
12. Abatzoglou, J.T.; Barbero, R.; Nauslar, N.J. Diagnosing Santa Ana Winds in Southern California with synoptic-scale analysis. *Weather. Forecast.* **2013**, *28*, 704–710. [CrossRef]
13. Rolinski, T.; Capps, S.B.; Zhuang, W. Santa Ana Winds: A Descriptive Climatology. *Weather. Forecast.* **2019**, *34*, 257–275. [CrossRef]
14. Cal Fire Top 20 Most Destructive California Wildfires. Available online: https://www.fire.ca.gov/stats-events/ (accessed on 5 December 2019).
15. Monteverdi, J.P. The Santa Ana Weather Type and Extreme Fire Hazard in the Oakland-Berkeley Hills. *Weatherwise* **1973**, *26*, 118–121. [CrossRef]
16. Bowers, C.L. The Diablo Winds of Northern California. Master's Thesis, San Jose State University, San Jose, CA, USA, December 2018.
17. Smith, C.; Hatchett, B.; Kaplan, M. A Surface Observation Based Climatology of Diablo-Like Winds in California's Wine Country and Western Sierra Nevada. *Fire* **2018**, *1*, 25. [CrossRef]
18. Werth, P.A.; Potter, B.E.; Alexander, M.E.; Clements, C.B.; Cruz, M.G.; Finney, M.A.; Forthofer, J.M.; Goodrick, S.L.; Hoffman, C.; McAllister, S.S.; et al. *Synthesis of Knowledge of Extreme Fire Behavior: Volume I for Fire Managers*; USDA Forest Service: Portland, OR, USA, 2011; 144p.
19. Camp Fire. Available online: https://www.fire.ca.gov/incidents/2018/11/8/camp-fire/ (accessed on 20 April 2018).
20. Cal Fire. *Camp Incident Green Sheet*; California Department of Forestry and Fire Protection: Sacramento, CA, USA, 2018.

21. Cooperative Distributed Interactive Atmospheric Catalog System/Earth Observing Laboratory/National Center for Atmospheric Research/University Corporation for Atmospheric Research, and Climate Prediction Center/National Centers for Environmental Prediction/National Weather Service/NOAA/U.S. Department of Commerce. *NCEP/CPC Four Kilometer Precipitation Set, Gauge and Radar*; Research Data Archive at the National Center for Atmospheric Research; Computational and Information Systems Laboratory: Boulder, CO, USA, 2000. [CrossRef]
22. Advanced Hydrologic Prediction Service. Available online: https://water.weather.gov/precip/download.php (accessed on 24 March 2018).
23. Zachariassen, J.; Zeller, K.; Nikolov, N.; McClelland, T. *A Review of the Forest Service Remote Automated Weather Station (RAWS) Network*; Gen. Tech. Rep. RMRS-GTR; USDA Forest Service: Fort Collins, CO, USA, 2003; pp. 1–161.
24. Cohen, J.D.; Deeming, J.E. *The National Fire-Danger Rating System: Basic Equations*; Gen. Tech. Rep. PSW-82; USDA Forest Service: Berkeley, CA, USA, 1985; p. 16.
25. Deeming, J.E.; Burgan, R.E.; Cohen, J.D. *National Fire-Danger Rating System*; Dept. of Agriculture, Forest Service, Intermountain Forest and Range Experiment Station: Ogden, UT, USA, 1978.
26. University of Wyoming Atmospheric Sounding. Available online: http://weather.uwyo.edu/upperair/sounding.html (accessed on 5 June 2018).
27. Clements, C.B.; Oliphant, A.J. The California State University Mobile Atmospheric Profiling System: A Facility for Research and Education in Boundary Layer Meteorology. *Bull. Am. Meteorol. Soc.* **2014**, *95*, 1713–1724. [CrossRef]
28. NOAA National Weather Service (NWS) Radar Operations Center. *NOAA Next Generation Radar (NEXRAD) Level 2 Base Data*; KBBX, NOAA National Centers for Environmental Information: Asheville, NC, USA, 1991. [CrossRef]
29. Environmental Modeling Center. *National Centers for Environmental Prediction*; National Weather Service, NOAA, U.S. Department of Commerce: College Park, MD, USA, 2018.
30. Skamarock, W.C.; Klemp, J.B.; Dudhia, J.; Gill, D.O.; Barker, D.M.; Duda, M.G.; Huang, X.Y.; Wang, W.; Powers, J.G. *A Description of the Advanced Research WRF Version 3*; NCAR Technical Note TN-475+ STR; National Center for Atmospheric Research: Boulder, CO, USA, 2008.
31. Mesinger, F.; Kalnay, E.; Mitchell, K.; Shafran, P.C.; Ebisuzaki, W.; Jovi'c, D.; Woollen, J.; Rogers, E.; Berbery, E.H.; Ek, M.B.; et al. North American Regional Reanalysis. *Bull. Am. Meteorol. Soc.* **2006**, *87*, 343–360. [CrossRef]
32. Cao, Y.; Fovell, R.G. Downslope windstorms of San Diego County. Part I: A Case Study. *Mon. Weather Rev.* **2016**, *144*, 529–552. [CrossRef]
33. Cao, Y.; Fovell, R.G. Downslope Windstorms of San Diego County. Part II: Physics Ensemble Analyses and Gust Forecasting. *Weather Forecast.* **2018**, *33*, 539–559. [CrossRef]
34. Fovell, R.; Gallagher, A. Winds and Gusts during the Thomas Fire. *Fire* **2018**, *1*, 47. [CrossRef]
35. Pleim, J.E.; Xiu, A. Development and testing of a surface flux and planetary boundary layer model for application in mesoscale models. *J. Appl. Meteorol.* **1995**, *34*, 16–32. [CrossRef]
36. Pleim, J.E. A combined local and nonlocal closure model for the atmospheric boundary layer. Part I: Model description and testing. *J. Appl. Meteorol. Climatol.* **2007**, *46*, 1383–1395. [CrossRef]
37. Appenzeller, C.; Davies, H. Structure of stratospheric intrusions into the troposphere. *Nature* **1992**, *358*, 570–572. [CrossRef]
38. McIntyre, M.E.; Palmer, T.N. The 'surf zone' in the stratosphere. *J. Atmos. Terr. Phys.* **1984**, *46*, 825–849. [CrossRef]
39. McIntyre, M.E.; Palmer, T.N. Breaking planetary waves in the stratosphere. *Nature* **1983**, *305*, 593–600. [CrossRef]
40. Albini, F.A. *Estimating Wildfire Behavior and Effects*; Gen. Tech. Rep. INT-30; USDA Forest Service: Ogden, UT, USA, 1976; p. 64.
41. Cheney, N.P.; Gould, J.S. Fire Growth in Grassland Fuels. *Int. J. Wildland Fire* **1995**, *5*, 237–247. [CrossRef]